

Current-dependent positive magnetoresistance in $La_{0.8}Ba_{0.2}MnO_3$ ultrathin films

Guankai Lin(林冠凯), Haoru Wang(王昊儒), Xuhui Cai(蔡旭晖), Wei Tong(童伟), and Hong Zhu(朱弘)
Citation: Chin. Phys. B, 2021, 30 (**9**): 097502. DOI: 10.1088/1674-1056/ac012d
Journal homepage: http://cpb.iphy.ac.cn; http://iopscience.iop.org/cpb

What follows is a list of articles you may be interested in

Emergent O(4) symmetry at the phase transition from plaquette-singlet to antiferromagnetic order in quasi-two-dimensional quantum magnets

Guangyu Sun(孙光宇), Nvsen Ma(马女森), Bowen Zhao(赵博文), Anders W. Sandvik, and Zi Yang Meng(孟子杨)
Chin. Phys. B, 2021, 30 (**6**): 067505. DOI: 10.1088/1674-1056/abf3b8

Magnetization and magnetic phase diagrams of a spin-1/2 ferrimagnetic diamond chain at low temperature

Tai-Min Cheng(成泰民), Mei-Lin Li(李美霖), Zhi-Rui Cheng(成智睿), Guo-Liang Yu(禹国梁), Shu-Sheng Sun(孙树生), Chong-Yuan Ge(葛崇员), and Xin-Xin Zhang(张新欣)
Chin. Phys. B, 2021, 30 (**5**): 057503. DOI: 10.1088/1674-1056/abd768

Crystal structure and electromagnetic responses of tetragonal GdAlGe

Cong Wang(王聪), Yong-Quan Guo(郭永权), Tai Wang(王泰), and Shuo-Wang Yang(杨硕望)
Chin. Phys. B, 2020, 29 (**12**): 127502. DOI: 10.1088/1674-1056/abad25

Colossal magnetoresistance in manganites and related prototype devices

Liu Yu-Kuai, Yin Yue-Wei, Li Xiao-Guang
Chin. Phys. B, 2013, 22 (**8**): 087502. DOI: 10.1088/1674-1056/22/8/087502

Reactively sputtered Fe_3O_4-based films for spintronics

Li Peng, Jin Chao, Mi Wen-Bo, Bai Hai-Li
Chin. Phys. B, 2013, 22 (**4**): 047505. DOI: 10.1088/1674-1056/22/4/047505

Current-dependent positive magnetoresistance in $La_{0.8}Ba_{0.2}MnO_3$ ultrathin films*

Guankai Lin(林冠凯)[1], Haoru Wang(王昊儒)[1], Xuhui Cai(蔡旭晖)[1], Wei Tong(童伟)[2], and Hong Zhu(朱弘)[1,3,†]

[1] *Department of Physics, University of Science and Technology of China, Hefei* 230026, *China*
[2] *Anhui Province Key Laboratory of Condensed Matter Physics at Extreme Conditions, High Magnetic Field Laboratory of the Chinese Academy of Sciences, Hefei* 230031, *China*
[3] *Key Laboratory of Strongly-Coupled Quantum Matter Physics, Chinese Academy of Sciences, Hefei* 230026, *China*

(Received 24 March 2021; revised manuscript received 8 May 2021; accepted manuscript online 14 May 2021)

We report an investigation into the magnetoresistance (MR) of $La_{0.8}Ba_{0.2}MnO_3$ ultrathin films with various thicknesses. While the 13 nm-thick film shows the commonly reported negative magnetoresistive effect, the 6 nm- and 4 nm-thick films display unconventional positive magnetoresistive (PMR) behavior under certain conditions. As well as the dependence on the film's thickness, it has been found that the electrical resistivity and the PMR effect of the thinner films are very dependent on the test current. For example, the magnetoresistive ratio of the 4 nm-thick film changes from +46% to −37% when the current is increased from 10 nA to 100 nA under 15 kOe at 40 K. In addition, the two thinner films present opposite changes in electrical resistivity with respect to the test current, i.e., the electroresistive (ER) effect, at low temperatures. We discuss the complex magnetoresistive and ER behaviors by taking account of the weak contacts at grain boundaries between ferromagnetic metallic (FMM) grains. The PMR effect can be attributed to the breaking of the weak contacts due to the giant magnetostriction of the FMM grains under a magnetic field. Considering the competing effects of the conductive filament and local Joule self-heating at grain boundaries on the transport properties, the dissimilar ER effects in the two thinner films are also understandable. These experimental findings provide an additional approach for tuning the magnetoresistive effect in manganite films.

Keywords: positive magnetoresistance, electroresistance, Joule self-heating, conductive filament

PACS: 73.43.Qt, 84.37.+q, 52.50.Nr, 52.38.Hb **DOI:** 10.1088/1674-1056/ac012d

1. Introduction

In recent decades, the colossal magnetoresistive (CMR) effect in perovskite manganites has attracted extensive attention because of its potential application in magnetic recording and sensors.[1–3] It has also been widely recognized that the double-exchange interaction between $Mn^{3+/4+}$ ions is a key mechanism that is responsible for the significant decrease of the electrical resistance under a magnetic field at temperatures around the magnetic phase transition.[4] However, in manganites, a positive magnetoresistive (PMR) effect, i.e., a magnetic-field-induced increase of resistance, has not been reported as frequently as colossal magnetoresistance. Some researchers have observed the PMR effect in manganite p-n heterostructures near room temperature.[5–7] For example, Jin *et al.* observed magnetoresistance under low applied magnetic fields and at high temperatures in a $La_{0.9}Sr_{0.1}MnO_3/SrNb_{0.01}Ti_{0.99}O_3$ p–n junction, and they proposed that the creation of a space-charge region at the interface was the PMR mechanism.[5] Other researchers have reported the PMR phenomenon in phase-separated manganites at low temperatures.[8–11] Chen *et al.* observed magnetoresistance in a single crystal of $La_{0.7}PbMnO_3$ at temperatures between 4.2 K and 50 K and attributed it to the quantum interference effect.[8] Because of the high diversity and complexity of the reported results, more detailed investigations are needed to understand the PMR phenomenon in manganites.

In addition to the magnetic-field effects, many works have also focused on current effects, such as electroresistance,[12–14] Joule self-heating,[15,16] and current-modulated magnetoresistance (MR)[17–20] due to their applications in storage devices and key devices for neuromorphic computing.[21] Yang *et al.* found a current dependence of low-field MR in single-crystal bilayer $La_{1.2}Sr_{1.8}Mn_2O_7$, and interpreted the phenomenon using a framework of percolating conduction and a local Joule thermal effect.[17] Gao *et al.* also reported a current-induced change in MR, which was attributed to phase separation and a current-induced metal–insulator transition in their $La_{0.8}Ca_{0.2}MnO_3$ thin film.[18] Although those authors observed current-modulated MR, the MR ratio always remained negative in their results. So far, the sign reversal of MR induced by a test current has rarely been reported in the literature. In this paper, we report a large PMR effect in 4 nm- and 6 nm-thick $La_{0.8}Ba_{0.2}MnO_3$ (LBMO) ultrathin films at low temperatures at a test current of 10 nA. When the current is increased to 100 nA, the MR ratio changes from positive to negative. Considering the existence of a large number of ferromagnetic metallic (FMM) grains in the ultra-

*Project supported by the National Natural Science Foundation of China (Grant No. 11674298), the National Key Research and Development Program of China (Grant No. 2017YFA0403502), and the Users with Excellence Project of Hefei Science Center CAS (Grant No. 2018HSC-UE013).

†Corresponding author. E-mail: zhuh@ustc.edu.cn

© 2021 Chinese Physical Society and IOP Publishing Ltd

thin films, the PMR effect can be understood as breaking the weak contacts between the FMM grains due to their giant negative magnetostriction under magnetic fields. Furthermore, changes of the weak contacts at various test currents play a key role to the sign reversal of the MR ratio.

2. Experimental details

We deposited $La_{0.8}Ba_{0.2}MnO_3$ thin films on $LaAlO_3$ (001) single-crystal substrates by the sol-gel method. Citric acid, $Mn(NO_3)_2{\cdot}4H_2O$, $La(NO_3)_3{\cdot}6H_2O$, and $Ba(NO_3)_2$ powder were dissolved in a mixed solvent of H_2O and ethylene glycol (1:1) using a magnetic stirrer at 60 °C for 2 h to form a homogeneous solution (with 0.16 mol/L of manganese ions). The sol was then deposited by a dip-coating process with pulling speeds of 8 mm/min, 1.2 mm/min, and 1 mm/min to obtain films with the thicknesses of 13 nm, 6 nm, and 4 nm, respectively. The samples were then heated at 100 °C for 10 min in air to drive off the water. Finally, they were heated to 850 °C to remove organic matter and crystallize the films.

Because the lattice parameter of the LBMO bulk (3.894 Å) is larger than that of the LAO substrate (3.79 Å), an in-plane compressive strain was expected in the LBMO epitaxial films, corresponding to an elongated out-of-plane lattice. X-ray diffraction (XRD) patterns revealed that the samples were single-phase and (001)-oriented films, as shown in our previous work.[22] Contrary to expectations, however, the out-of-plane lattice parameter was slightly smaller than the bulk value. In addition, scanning electron microscope (SEM) images showed a nano-sized labyrinth morphology rather than a smooth and uniform surface. Therefore, we concluded that the LBMO/LAO thin films were strain-relaxed incompact films. The film thicknesses were measured using atomic force microscopy (AFM). Because the substrates were not completely covered by the films, the film thicknesses were derived from the step height between the film and the substrate. The electrical transport properties and resistance–current curves were measured using a nanovoltmeter (Keithley 2182A) and a current source (Keithley 6221). The measurements were carried out using a linear four-probe configuration with an electrode length of 7 mm and an electrode separation of 2 mm, respectively. The electrical contacts were made using silver paste. The measurements were carried out from 10 K to 300 K in a Janis cryostat (SHI-4-2) coupled with a Lakeshore 340 temperature controller. The temperature-dependent magnetization $M(T)$ was measured using a vibrating sample magnetometer (Quantum Design MPMS). The magnetoresistance measurement was performed using a physical properties measurement system (Quantum Design PPMS).

3. Results and discussion

Figures 1(a) and 1(b) show the temperature-dependent resistivity and magnetization of the 13 nm- and 6 nm-thick LBMO films. In the case of the 13 nm-thick film, it can be seen that a metal–insulator transition (MIT) occurs at 260 K, accompanied by a ferromagnetic transition at the Curie temperature $T_C \sim 270$ K. The coincidence of the MIT temperature T_P and the Curie point T_C is a common feature of doped manganites, especially large-bandwidth manganites with Sr and Ba substitution at the A site. In Fig. 1(b), the 6 nm-thick film shows a fairly low MIT temperature T_P of 97 K, while the Curie temperature T_C remains unchanged. In narrow-bandwidth manganites, such a discrepancy between T_P and T_C is usually regarded as a sign of electronic phase separation. However, this does not seem to be the case in this work, because our samples are wide-bandwidth films with inappreciable strain. Furthermore, the unchanged T_C suggests that the double exchange interaction is little changed in the thinner film. Therefore, phase separation arising from reduced e_g electron hopping and suppressed double exchange can be ruled out. In previous work, the effects of grain size on the electrical and magnetic properties of manganites have been reported by many authors.[23–25] Dey *et al.* observed a gradual drop of the MIT temperature with a decrease in the grain size, while the ferromagnetic–paramagnetic transition temperature remained almost unchanged in their granular $La_{0.7}Ca_{0.3}MnO_3$ samples.[23] Here, we consider the grain size effect to be the reason for the much lower T_P in the 6 nm-thick film. In fact, the morphology and microstructure of manganite films might depend on the film thickness.[26] Arun *et al.* found that the long-range ferromagnetic order in the $Nd_{0.67}Sr_{0.33}MnO_3$ manganites becomes unstable when reducing the grain size down to nano-meter scale.[27] In the present work, because of the reduced thickness, the 6 nm-thick film must have smaller grains and wider size distribution. We note that the 6 nm-thick film shows a more slowly increased M–T curve with decreasing temperature than the thicker film does. It suggests a sustained and moderated transition from the paramagnetic insulating (PMI) state to the FMM state due to the wider distribution of the grain size. At temperatures just below $T_C \sim 270$ K, the FMM grains are not abundant enough to contact with each other, and thus the 6 nm-thick film displays an insulating transport behavior. With further decreasing temperature, some smaller grains gradually change to the FMM state. Eventually at $T_P \sim 97$ K, volume fraction of the FMM grains reaches the percolation threshold, corresponding to the sharp decrease in the ρ–T curve. As a contrast, the MIT temperature T_P of the 13 nm-thick film is just a little bit lower than the Curie temperature T_C, suggesting fairly consistent transitions in the grains with similar sizes. In addition, it is worth noting that the resistivity of the 6 nm-thick film is 3 orders of magnitude larger than that of the 13 nm-thick film as a whole. At low temperatures, the 6 nm-thick film shows a relatively high residual resistivity. These results imply that the grain boundary in the thinner film plays an important role in its transport properties.

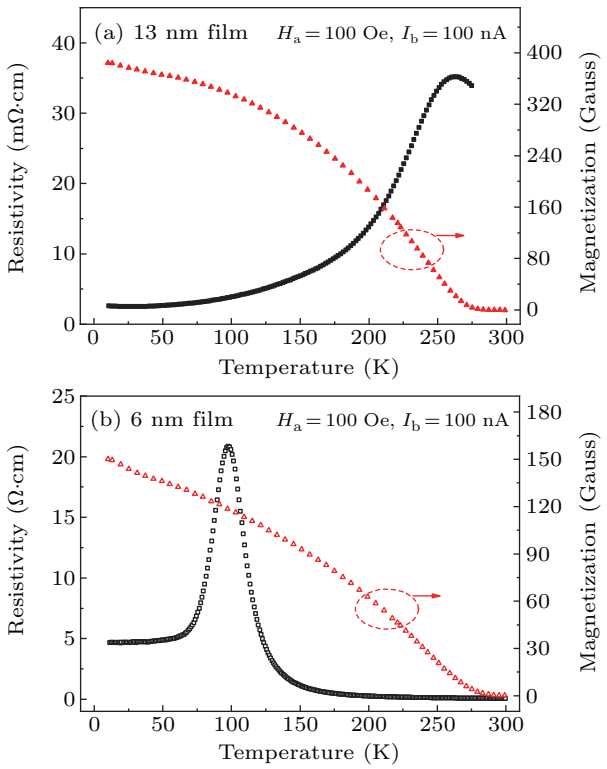


Fig. 1. Temperature dependence of the resistivity at the test current of $I_b = 100$ nA and field-cooled (FC at 3 kOe) magnetization of the 13 nm-thick film (a) and the 6 nm-thick film (b). The magnetic field is 100 Oe applied parallel to the film plane.

To investigate the grain boundary effect in the thinner LBMO film, the current dependence of the electroresistive (ER) ratio, which is defined as $(R(I) - R(10\text{ nA}))/R(10\text{ nA}) \times 100\%$, was measured at various temperatures, as shown in Fig. 2. The current was swept from 10 nA to 100 nA at a rate of 1 nA/s. At temperatures above T_P, i.e., 120 K, it can be seen that the 6 nm-thick film has an almost zero ER ratio, suggesting current independent transport behavior. When the temperature is decreased to 65 K (below T_P), the thinner film shows a negative ER ratio of $\sim 25\%$ at 100 nA, corresponding to a reduction in the resistivity under an electric current/field. With a further decrease of the temperature to 40 K, the ER ratio even increases to $\sim 60\%$. The evolution of the ER behavior with respect to temperature can be understood by taking the FMM grains into account. At temperatures above T_P, the FMM grains are relatively few and distant from each other, so that the resistivity of the thinner film is governed by the PMI grains. Hence, the applied current has little impact on the transport behavior. When the thinner film is cooled to temperatures below T_P, the FMM grains increase in size and contact each other, resulting in a sharp decline in the resistivity, as shown in Fig. 1(b). More importantly, some boundaries between FMM grains become quite narrow. Under these conditions, conductive filaments can form in the narrow boundaries under an electric current/field because of the migration of oxygen vacancies,[21,28] which in turn results in a reduction of the resistivity, i.e., negative electroresistance in the thinner LBMO film. With a further decrease of the temperature to 40 K, more FMM grains appear in the thinner film, and the increased number of boundaries promotes the emergence of conductive filaments, resulting in enhanced electroresistance at the lower temperature. For comparison, the current dependence of the ER ratio of the 13 nm-thick film was also measured. In Fig. 2, the thicker film shows a negligible ER effect, even at 40 K, while the thinner film has the largest ER ratio. At higher temperatures, the resistivity of the 13 nm-thick film still presents current-independent behavior (not shown here). From another perspective, this demonstrates again that the grain boundary in the thinner film is one of the key factors to its transport properties.

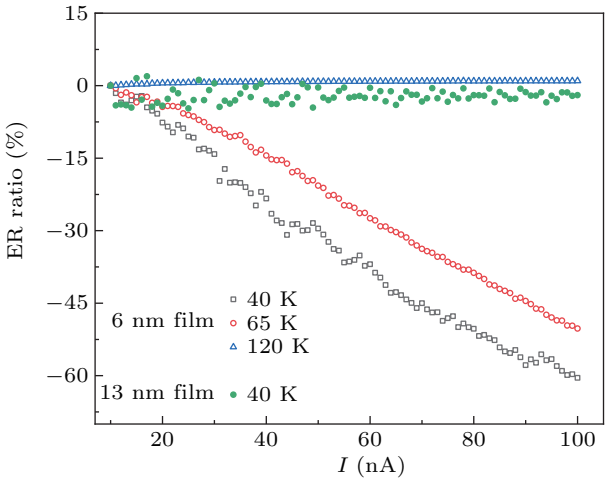


Fig. 2. ER ratio as a function of the test current for the 6 nm-thick film at 40 K, 65 K, and 120 K, respectively and for the 13 nm-thick film at 40 K.

While intrinsic colossal magnetoresistance in doped manganites is restricted to a temperature range at around their transition temperatures, a grain boundary usually gives rise to a negative magnetoresistive effect at low temperatures because of spin-dependent tunneling between the FMM grains.[27,29,30] To shed more light on the grain-boundary effect, we measured the magnetic field-dependent resistivity for the two films at low temperatures. The magnetic field perpendicular to the film plane was first increased from 0 to 15 kOe, and the measurement data were then recorded while sweeping the magnetic field from 15 kOe to −15 kOe. Figure 3(a) shows the results measured at a test current of 100 nA. For the 13 nm-thick film at 40 K, the resistivity decreases monotonically with an increase in the applied magnetic field up to 15 kOe, corresponding to a magnetoresistive ratio $\sim 7\%$. It can be considered to be a result of the small number of grain boundaries in the thicker film. By contrast, the 6 nm-thick film shows a larger negative magnetoresistive ratio of $\sim 23\%$ at 120 K, suggesting a larger grain-boundary effect, which is inconsistent with the ER data mentioned above. At 40 K, the thinner film shows a negative MR as normal under the magnetic field below 7.5 kOe. With a further increase in the magnetic field, however, it is interesting that an abnormal upturn in the resistivity can be observed, suggesting a PMR behavior in the thinner film.

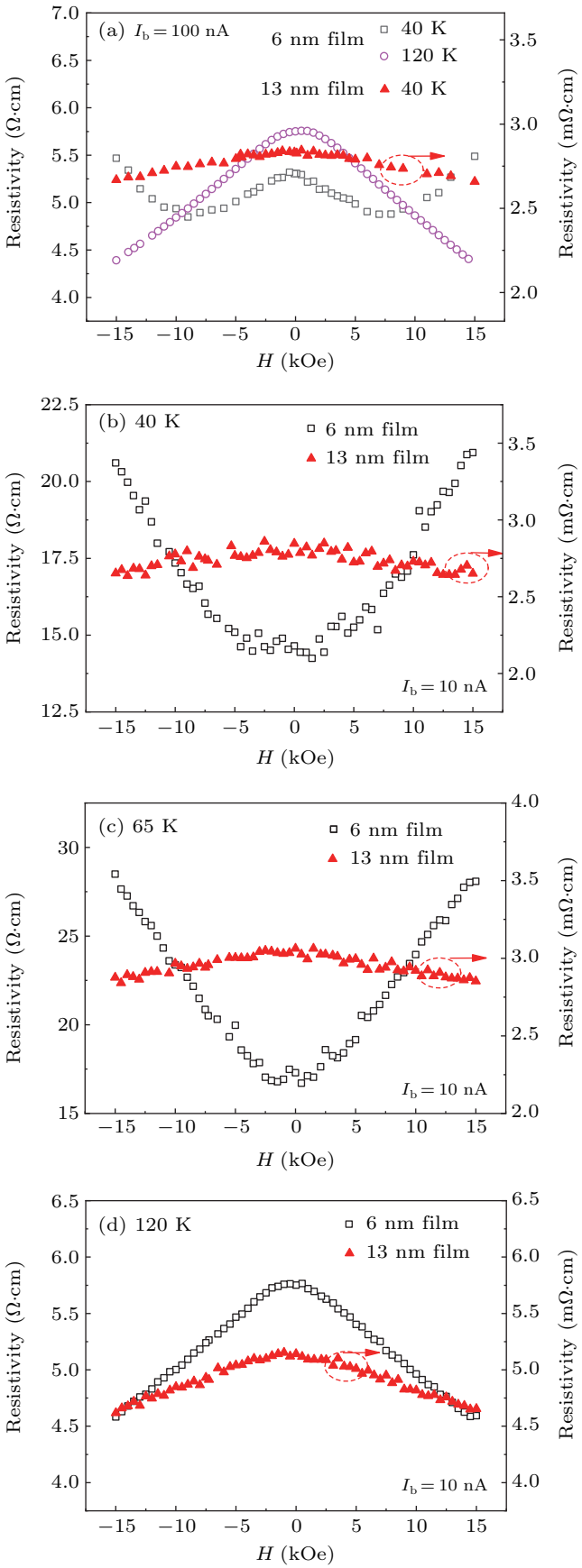


Fig. 3. (a) Magnetic field dependence of the resistivity for the 13 nm-thick film at 40 K and the 6 nm-thick film at 40 K and 120 K, respectively. The test current is 100 nA. (b)–(d) Magnetic field dependence of the resistivities of the 13 nm- and 6 nm-thick films at 40 K, 65 K, and 120 K, respectively. The test current I_b is 10 nA. The magnetic field is applied perpendicular to the film plane.

Considering that the 6 nm-thick film exhibited a current-dependent resistivity at lower temperatures, we measured the magnetic-field dependence of the resistivity at a lower test current of 10 nA for the 6 nm-thick film as well as the 13 nm-thick film for comparison. Figures 3(b)–3(d) display the ρ–H curves measured at 40 K, 65 K, and 120 K, respectively. The 13 nm-thick film gives an almost unchanged negative MR ratio $\sim 7\%$ under 15 kOe at various temperatures, although the data measured at 40 K are somewhat scattered because of the weak voltage signals. This is in agreement with the zero ER result for the thicker film. However, the 6 nm-thick film displays a complex magnetoresistive behavior, which is dependent not only on the test current but also on temperature. At 40 K, figure 3(b) shows that the thinner film behaves in a completely PMR way, with a PMR ratio of $\sim 45\%$ at 15 kOe. When the temperature is increased to 65 K, as shown in Fig. 3(c), the PMR ratio at 15 kOe increases to $\sim 70\%$, suggesting a significantly enhanced PMR effect in the thinner film. Finally, at 120 K, the 6 nm-thick film presents a negative magnetoresistive behavior over the whole of the measured range, as shown in Fig. 3(d), with a magnetoresistive ratio of $\sim 23\%$ at 15 kOe, which is almost the same as the value measured at 100 nA.

It is now clear that the 13 nm-thick film displays a current-independent weak negative magnetoresistive effect at lower temperatures because of the commonly reported spin-dependent tunneling across grain boundaries.[27,29,30] However, the 6 nm-thick film shows various aspects of the magnetoresistive effect. Here, we consider that the electrical contact between FMM grains plays a key role. At 120 K, which is higher than the MIT temperature T_P, the FMM grains do not touch each other, so the thinner film simply gives a negative magnetoresistive effect, as normal. Because the thinner film has more FMM grains with smaller sizes, its magnetoresistive ratio is larger than that of the 13 nm-thick film, as shown in Fig. 3(d). At 65 K and 40 K below T_P, the thinner film displays the PMR effect, which has rarely been observed in doped manganites. Endo *et al.* reported a similar PMR behavior in $La_{0.7}Ba_{0.3}MnO_3$ films epitaxially grown on $LaAlO_3$ substrates by the ion beam sputtering technique,[31] but its dependence on the test current was not mentioned. We note that some authors have reported a giant (volume) magnetostrictive effect in doped manganites with a coefficient of $\sim -10^{-4}$,[32–35] while it is around 10^{-5} in conventional ferromagnetic materials. In addition, Ba-doped manganites show much larger negative magnetostriction than their Sr- and Ca-doped counterparts.[33] According to these conclusions, in the present work, we speculate that the PMR effect might result from the giant negative magnetostriction of the FMM grains. When the temperature decreases below T_P, the number of FMM grains increases and they come into contact with each other, resulting in a decline in the resistivity. However, the

newly-established contacts are fragile. Under the applied magnetic field, volumetric shrinkage of the FMM grains occurs due to the negative magnetostrictive effect. As a result, the weak contacts of the FMM grains begin to disconnect, giving rise to the PMR behavior observed in the thinner film. At the higher temperature of 65 K, the contacts are even worse, so the 6 nm-thick film has a higher PMR ratio of ∼ 70% than the value of 45% at 40 K, as shown in Figs. 3(b) and 3(c). At the higher test currents of 100 nA and 40 K, the thinner film displays negative magnetoresistive and PMR behaviors when exposed to magnetic fields below and above 7.5 kOe respectively, as shown in Fig. 3(a). Because of the large ER effect in the thinner film, we consider that the higher current enhances the contacts between FMM grains, so that the film shows a normal negative magnetoresistive effect under magnetic fields of less than 7.5 kOe. With an increase in the magnetic field above a value of 7.5 kOe, the magnetic field is high enough to break the contacts, resulting in PMR behavior in the thinner film.

So far, it has been found that the magnetoresistive effect in LBMO films is closely related to the film thickness. To more fully investigate the influence of film thickness on the magnetoresistive effect, we further decreased the film thickness to 4 nm. The temperature-dependent resistivity and magnetization of the 4 nm-thick film are shown in Fig. 4(a). It can be seen that both its T_P (78 K) and T_C (250 K) decrease a little (∼ 20 K), compared to those of the 6 nm film, suggesting finer FMM grains in the thinnest film. We note that the resistivity at temperatures below T_P is almost one order of magnitude larger than that in the 6 nm film (shown in Fig. 1(b)), implying even worse electric contacts between the FMM grains than those in the thicker film.

We also measured the magnetic-field dependence of the resistivity for the 4 nm-thick film under a magnetic field perpendicular to the film plane at various temperatures and test currents, as shown in Figs. 4(b)–4(d). At 40 K in Fig. 4(b), the 4 nm-thick film shows some differences compared to the thicker 6 nm film. First, it can be seen that the resistivity under a zero magnetic field increases when the test current is increased from 1 to 100 nA, suggesting a positive ER effect, which is in stark contrast to the 6 nm-thick film. While the electric current/field induced conductive filaments are beneficial to the electric transport, we consider that local Joule self-heating at the weak contacts plays a negative role. It has been reported that Joule self-heating breaks the weak contacts between the FMM grains, but leads to a negligible change in the sample's temperature.[17,36] Because of the much higher low-temperature resistivity of the 4 nm-thick film, the negative effect of local Joule self-heating on the transport properties is larger than the positive effect of the conductive filaments, thus resulting in an increase in resistivity with increasing

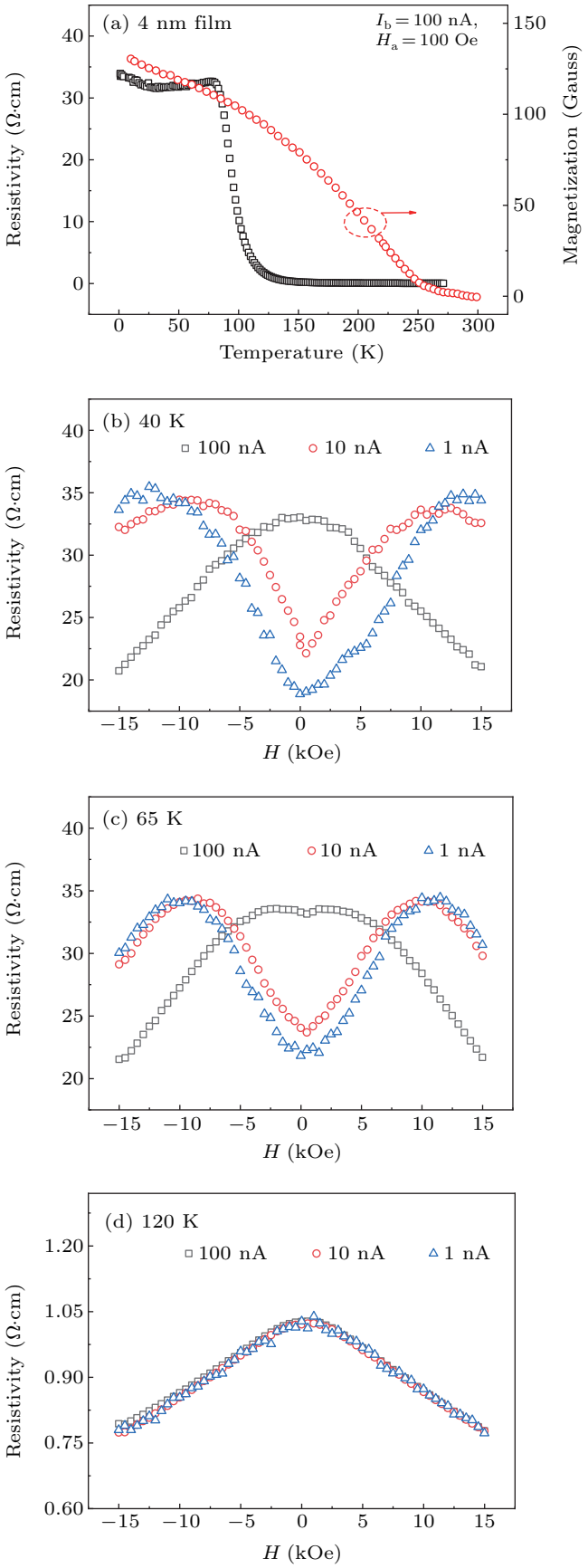


Fig. 4. (a) Temperature dependence of the resistivity at a test current of $I_b = 100$ nA and field-cooled magnetization for the 4 nm-thick film. The magnetic field is 100 Oe applied parallel to the film plane. (b)–(d) Magnetic field dependence of the resistivity for different test currents of the 4 nm-thick film at 40 K, 65 K, and 120 K respectively. The applied magnetic field is perpendicular to the film plane.

test current. Second, the resistivity at currents of less than 100 nA shows a continuous decrease with increasing magnetic fields of up to 15 kOe, rather than the upturn at 7.5 kOe in the 6 nm-thick film shown in Fig. 3(a). This means that the larger Joule self-heating caused by the higher current already breaks most of the weak contacts between the FMM grains, hence the 4 nm-thick film shows a commonly observed negative MR due to spin-dependent tunneling. Third, the resistivities at less than both 1 nA and 10 nA display a positive magnetoresistance under magnetic fields of les than $\sim$ 10 kOe, followed by negative MR with a further increase in the magnetic field. An explanation is that the lower Joule self-heating powers only break a small number of the weak contacts, and the volumetric shrinkage of the FMM grains under a magnetic field then further breaks the weak contacts, which in turn results in positive magnetoresistance under lower magnetic fields. When the magnetic field reaches $\sim$ 10 kOe, almost all of the weak contacts are broken, so the resistivities show a turning point to negative MR.

Another point worth noting in Fig. 4(b) is that the magnetic field ($\sim$ 13.5 kOe) corresponding to the MR turning point under 1 nA is higher than that ($\sim$ 12 kOe) at 10 nA. This implies that more weak contacts remain in the thinnest film under a lower test current (1 nA), so that a higher magnetic field is needed to break them. Under 15 kOe, it is also interesting that the resistivity decreases when the test current is increased, corresponding to a negative electroresistance, which is totally opposite to the positive electroresistance under a zero magnetic field. Because all the weak contacts are broken due to the magnetostriction of the FMM grains under high magnetic fields, Joule self-heating can do little to break the contacts between FMM grains. On the other hand, the electric current/field induced conductive filament plays a bigger role in this case, resulting in negative electroresistance under high magnetic fields.

When the temperature is increased to 65 K, the 4 nm-thick film displays similar ρ–H curves in Fig. 4(c) to those at 40 K. The major difference is that the magnetoresistive turning points at 1 nA and 10 nA occur at magnetic field strengths slightly lower than the corresponding values at 40 K. Because the FMM grains decrease in number at the higher temperature, it is reasonable that the worse contacts are broken under a lower magnetic field. With a further increase in temperature to 120 K, shown in Fig. 4(d), the 4 nm-thick film shows almost identical negative magnetoresistive behaviors at various test currents, implying that the FMM grains are totally separated and that the current effect on the electric transport of the insulating matrix is negligible.

We have now seen that the transport properties of LBMO films, especially the ultrathin films, is strongly dependent on the evolution of weak contacts between FMM grains with respect to temperature, magnetic field, and test current. With an increase in their numbers at low temperatures, the FMM grains start to touch each other, allowing percolating conduction in the films. Because of the small grain size, the electrical contacts between the FMM grains must be weak and subtle. Under an applied magnetic field, the volumetric shrinkage of the FMM grains due to the giant magnetostrictive effect breaks the weak contacts, leading to positive magnetoresistance. The test current has two contrary effects on the weak electrical contacts. One is the current-induced conductive filaments in the grain boundaries when the contacts are not too bad, resulting in a negative ER response in the 6 nm-thick film. The other is local Joule self-heating at grain boundaries, leading to the melting of weak contacts in the case of the poorer contacts, as demonstrated by the 4 nm-thick film. Because of the unique role of the weak contact/grain boundary between the FMM grains, the LBMO ultrathin films exhibit multiple electro- and magnetoresistive phenomena. Further investigation of these phenomena might confirm that they are promising candidates for use in memory devices and magnetic-field sensors.

4. Conclusion

In summary, we have investigated the magnetoresistive effect of $La_{0.8}Ba_{0.2}MnO_3$ ultrathin films with various thicknesses. A remarkable PMR phenomenon is found in the 6 nm- and 4 nm-thick films, which also show a large ER effect at low temperatures. The ER effect reveals that the weak contact/grain boundary between FMM grains plays an important role in the transport properties of ultrathin LBMO films. The PMR behavior can be attributed to the breaking of weak contacts, due to volumetric shrinkage of the FMM grains due to giant magnetostriction in Ba-doped manganites. It is interesting that the PMR ratio becomes negative under higher test currents or at temperatures above T_p. The magnetoresistive ratio of the 4 nm-thick film at 40 K under 15 kOe changes from $+46\%$ to -37% when the test current is increased from 10 nA to 100 nA. In addition, the two ultrathin films show opposite ER behaviors under a zero magnetic field. The complicated MR and ER manifestations are attributed to the contrary effects of the electric current/fieldinduced conductive filaments and local Joule-self heating at the grain boundaries. Our experimental results call for further investigation of the unconventional PMR effects in the LBMO ultrathin films, such as their anisotropic response to the applied magnetic field and the influence of oxygen deficiency in the films, especially at grain boundaries.

References

[1] Ramirez A P 1997 *J. Phys. : Condens. Matter* **9** 8171
[2] Li X Y, Zhao L and Wei X Y, *et al.* 2018 *Chin. Phys. B* **27** 117501

[3] Xiang P H, Zhong N, Sun L, Tang X D and Duan C G 2018 *J. Phys. D: Appl. Phys.* **51** 275304
[4] Zener C 1951 *Phys. Rev.* **82** 403
[5] Jin K J, Lu H B, Zhou Q L, *et al.* 2005 *Phys. Rev. B* **71** 184428
[6] Lu H B, Yang G Z, Chen Z H, *et al.* 2004 *Appl. Phys. Lett.* **84** 5007
[7] Khachar U D, Solanki P S, Choudhary R J, *et al.* 2012 *Appl. Phys. A* **108** 733
[8] Chen P, Xing D Y and Du Y W 2001 *Phys. Rev. B* **64** 104402
[9] Ziese M 2003 *Phys. Rev. B* **68** 132411
[10] Yun S H, Dhakal T, Goswami D, Singh G, Herbard A and Biswas A 2008 *J. Appl. Phys.* **103** 07E317
[11] Shaykhutdinov K A, Nikitin S E, Petrov M I, Terent'ev K I, Semenov S V and Popkov S I 2015 *J. Appl. Phys.* **117** 163918
[12] Wu T, Ogale S B, Garrison J E, Nagaraj B, Biswas A, Chen Z, Greene R L, Ramesh R and Venkatesan T 2001 *Phys. Rev. Lett.* **86** 5998
[13] Sun Y H, Zhao Y G and Wang R G 2017 *Chin. Phys. B* **26** 047103
[14] Lourembam J, Ding J F, Bera A, Lin W N and Wu T 2014 *Appl. Phys. Lett.* **104** 133508
[15] Nhalil H and Elizabeth S 2016 *Solid State Commun.* **248** 6
[16] Carneiro A S and Jardim R F 2006 *Phys. Rev. B* **73** 012410
[17] Yang R F, Sun Y, Ma X, Tang Y K, Li Q A and Cheng Z H 2006 *Phys. Rev. B* **73** 092404
[18] Gao J and Hu F X 2006 *Mater. Sci. Eng. B* **126** 250
[19] Kumar R, Gupta A K, Singh D P, Kumar V, Bhalla G L and Khare N 2008 *J. Magn. Magn. Mater.* **320** 2741
[20] Yang C P, Chen S S, Zhou Z H, Xu L F, Wang H, Hu J F, Morchshakov V and Bärner K 2007 *J. Appl. Phys.* **101** 063909
[21] Del Valle J, Ramírez J G, Rozenberg M J and Schuller I K 2018 *J. Appl. Phys.* **124** 211101
[22] Lin G K, Wang H R, Cai X H, Tong W and Zhu H 2020 *AIP Adv.* **10** 055206
[23] Dey P and Nath T K 2006 *Phys. Rev. B* **73** 214425
[24] Lim K P, Ng S W, Lau N L, *et al.* 2019 *Appl. Phys. A* **125** 745
[25] Skini R, Svedlindh P, Dhahri E, *et al.* 2019 *J. Mater. Sci. : Mater Electron* **30** 17363
[26] Zurauskiene N, Balevicius S, Stankevic V, *et al.* 2018 *J. Mater. Sci.* **53** 12996
[27] Arun B, Suneesh M V and Vasundhara M 2016 *J. Magn. Magn. Mater.* **418** 265
[28] Kwon D H, Kim K M, Jang J H, Jeon J M, Lee M H, Kim G H, Li X S, Park G S, Lee B, Han S, Kim M and Hwang C S 2010 *Nat. Nanotechnol.* **5** 148
[29] Sadhu A and Bhattacharyya S 2014 *Chem. Mater.* **26** 1702
[30] Phong P T, Bau L V, Hoan L C, *et al.* 2016 *J. Alloy. Comp.* **656** 920
[31] Endo T, Uehara K, Yoshii T, Yorkura M, Zhu H, Nogues J, Colino J and Endo K 2010 *Trans. Mat. Res. Soc. Jpn.* **35** 727
[32] Mahendiran R, Ibarra M R, Marquina C, Garcia-Landa B, Morellon L, Maignan A, Raveau B, Arulraj A and Rao C N R 2003 *Appl. Phys. Lett.* **82** 242
[33] Koroleva L I, Demin R V, Kozlov A V, Zashcherinskii D M, Gorbenko O Y, Kaul A R, Melnikov O V and Mukovskii Y M 2007 *J. Magn. Magn. Mater.* **316** e644
[34] Yazdi S T, Tajabor N and Khoshnoud D S 2010 *J. Magn. Magn. Mater.* **322** 3131
[35] Xu M H, Hu X K, Yu J Y, Cui X G and Zhang S Y 2008 *Solid State Commun.* **148** 217
[36] Tokunaga M, Tokunaga Y and Tamegai T 2004 *Phys. Rev. Lett.* **93** 037203